The electronic structure of f-element Prussian blue analogs determined by soft X-ray absorption spectroscopy

Thomas Dumas, Dominique Guillaumont, Philippe Moisy, David Shuh, Tolek Tyliszczak, Pier Lorenzo Solari, Christophe den Auwer

Title

The electronic structure of f-element Prussian blue analogs determined by soft X-ray absorption spectroscopy

Journal

Chemical Communications, 54(86)

ISSN

1359-7345

Authors

Dumas, Thomas

Guillaumont, Dominique

Moisy, Philippe

et al.

Publication Date

2018-10-25

DOI

10.1039/c8cc05176c

Peer reviewed

Journal Name

COMMUNICATION

Electronic structure of f-element Prussian Blue analogs determined by soft X-ray absorption spectroscopy.

Received 00th January 20xx,
Accepted 00th January 20xx

DOI: 10.1039/x0xx00000x

www.rsc.org/

Thomas Dumas*[a], Dominique Guillaumont[a], Philippe Moisy[a], David K. Shuh[b,c], Tolek Tyliszczak[c], Pier Solari[d] and Christophe Den Auwer[a,e]

In molecular solids derived from Prussian Blue, intermetallic charge transfer are fostered trough a cyano bridge between two transition metals. In this study, isostructural lanthanide and actinide Prussian Blue Analogs valence orbitals are probed by soft X-ray absorption measurements.

Bimetallic cyanide molecular solids derived from Prussian Blue are well known to exhibit remarkable electronic properties. It is also an interesting example of building block chemistry with structurally defined subfamilies. The d-block Prussian Blue Analogs (PBA) often present an intense intervalence charge transfer band (IVCT) arising from a short range exchange interaction through the cyano bridge between the two transition metal centers (Robin and Day class 2 behavior).[1] This family is broadly studied because of the remarkable electronic[2, 3] and magnetic[4] properties or for adsorption[5, 6] and ion exchange[6] applications tunable by exchanging the metal center type. The cyano-bridged PBA materials were synthesized with 3d, 4d, 5d transition metals as well as mixed nd/4f or nd/5f elements.[7] As for the d-block PBA members, PBA containing 5f and 4f are insoluble materials in aqueous solution and rapidly precipitate while mixing the hexacyanometallate precursor ($[M^{n+}(CN)_6]^{(6-n)-}$) with the targeted trivalent or tetravalent f-block elements. The synthesis and structural characterization for La^{3+}, Ce^{3+}, Nd^{3+}, Eu^{3+} Th^{4+}, U^{4+}, Np^{4+} and Pu^{4+} reacted with the ferrocyanide ($[Fe^{II}(CN)_6]^{4-}$) precursor were described previously. Structurally the 4f-PBA and 5f-PBA crystalize in either a hexagonal phase or orthorhombic phase depending on the f-element ionic radii. [8-17] For the early lanthanide and actinide series (Z < 60 and Z < 94, respectively), the hexagonal structure is preferred. The f-element sits in a tricapped trigonal prism site with 3 water molecules in the 3 capped planar positions and the 6 cyano ligands bridging to an octahedral iron site (see insert of Figure 1.a.).

Although early lanthanide and actinide PBA are isostructural, both optical and vibrational properties indicate distinct electronic behavior along the two series. The 4f-PBA exhibit pale colors almost equivalent to the corresponding Ln^{3+} ions in aqueous solution whereas the some of the 5f-PBA exhibit intense colors that distinguish from the corresponding ions. As an example, in Figure 1a, the UV-Vis absorption spectra for neodymium and neptunium aquo ions in solution (dashed lines) are compared to the corresponding PBA reflectance spectra (solid lines). For neodymium, the Nd^{3+} peaks remains almost unchanged in the Nd-PBA compound. In contrast, an

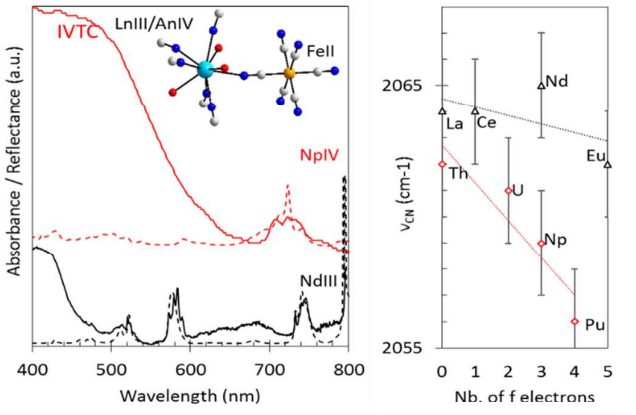

Figure 1 left: UV-Vis absorption spectra for neodymium and neptunium in aqueous solutions (black and red dotted line respectively) and the reflectance spectra for Nd-PBA and Np-PBA spectra (black and red full lines). Spectra are rescaled and offset vertically for clarity. Right: ν_{CN} stretching frequencies for the An-PBA and Ln-PBA as a function of the number of f electrons.

[a] CEA, Nuclear Energy Division, Radiochemistry and Process Department, 30207 Bagnols-sur-Cèze, France. E-mail: thomas.dumas@cea.fr.
[b] Chemical Sciences Division, Lawrence Berkeley National Laboratory, Berkeley, CA 94720, USA.
[c] Advanced Light Source Division, Lawrence Berkeley National Laboratory, LBNL, Berkeley, CA 94720, USA.
[d] Synchrotron SOLEILL'Orme des Merisiers, Saint-Aubin, BP 48F-91192, Gif-sur-Yvette Cedex, France
[e] Université Côte d'Azur, CNRS, Institut de Chimie de Nice, UMR 7272, 06108 Nice, France

Electronic Supplementary Information (ESI) available: [Hafnium ferrocyanide structural description]. See DOI: 10.1039/x0xx00000x

intense charge transfer band with a maximum at about 480 nm is observed for the Np-PBA spectrum.

These trends in optical properties distinguish the 4f-PBA from the 5f-PBA series for which IVTC bands may be observed. The IVCT is derived from an electronic exchange between the two metallic sites through the bridging cyano ligand and this suggests a different bonding mode between the 4f and 5f PBAs. Moreover, the bridging cyano ligand stretching frequencies also distinguish the 4f and 5f PBA series. In such cyano-bridged compounds, the CN bond strength is influenced by electronic exchange between the cyano σ molecular orbital, i.e., ligand metal charge transfer (LMCT), or back-bonding to the empty cyano π* molecular orbitals (MLCT). The ν_{CN} stretching frequencies for the An-PBA and Ln-PBA series are shown in Figure 1b (right) as a function of the number of f electrons. The 5f-PBAs are easily distinguished from the 4f-PBA based on ν_{CN} stretching frequencies. The ν_{CN} frequencies are almost stable for 4f-PBA's indicating little influence of the number of 4f electrons on the cyano ligand electronic structure. On the contrary, a significant variation is observed for the 5f-PBA. As the number of 5f electron increases, the ν_{CN} frequencies decreases indicating either, a decrease of electronic density in the bonding cyano σ molecular orbital or an increase in the electronic density in the anti-bonding cyano π* molecular orbitals.

Overall, vibrational and optical spectroscopy suggest distinctive electronic properties between 4f and 5f PBA but do not provide detailed electronic structure information. To determine more directly how the cyano ligand electronic structure is modified by bridging to 4f or 5f elements, soft X-ray absorption spectroscopy measurements were undertaken at the iron L_3 and nitrogen K edges. The spectroscopic measurements were performed in transmission mode at the ALS 11.0.2 beamline equipped with a Scanning Transmission X-ray Microscope suitable for radioactive samples.[18, 19] The N K and Fe L_3 edges from seven nf-PBA samples (ca., Ce-PBA, Nd-PBA, Eu-PBA, Th-PBA, U-PBA, Np-PBA, Pu-PBA) are displayed in Figure 2a and 2b respectively. $K_4[Fe(CN)_6]$ spectra (identical to previous work[20, 21]) are shown as a non-bridging cyano ligand reference. The same measurements made on a d-block tetravalent PBA analog (Hf-PBA) is shown in Fig. 1 for comparison. Hf-PBA crystalizes in a cmcm space group isomorphous to 4f-PBAs with Z > 63. EXAFS measurements (E.S.I.1) confirmed that the Hf4+ ions are 8 coordinated with 2 water molecules and 6 cyano ligands bridging to octahedral Fe2+ sites. This compound is structurally relevant for comparison to f-PBAs since both Fe2+ and CN- are orientated to form Fe-CN-Hf bridges geometrically similar to those in f-PBA compounds.

For $K_4[Fe(CN)_6]$, both the iron L_3 edge and nitrogen K edge spectra have been extensively studied.[20, 21] The $[Fe(CN)_6]^{4-}$ nitrogen K edge spectrum presents a single peak (A on Figure 2.a), with a maximum at 399.8 eV. This peak formally arises from $1s^2 2p^n \rightarrow 1s^1 2p^{n+1}$ dipolar transition. Considering the $K_4[Fe(CN)_6]$ electronic structure, only transitions to non-bonding cyano π* MOs and to t_{2g}* MOs (of 2p character) formed by the iron/cyano back bonding are observed (Figure 2c). The effect of back bounding is also directly seen on the other side of the PBA by the iron L_3 edge ($2p^6 3d^n \rightarrow 2p^5 3d^{n+1}$ dipolar transition). The octahedral ligand field effect that split the iron 3d orbitals into e_g and t_{2g} orbitals, further introduces 3d character into the 3 cyano π* MO's (t_{2g}* on Figure 2b.c) by the back bonding interactions. Hence, the two peaks arising at 710.1 eV and 711.5 eV are observed corresponding to transitions to e_g* and t_{2g}* MOs, respectively (B and C arrows on Figure 2.c) When ferrocyanides bridge to another metal, it is clear from both the nitrogen K and the

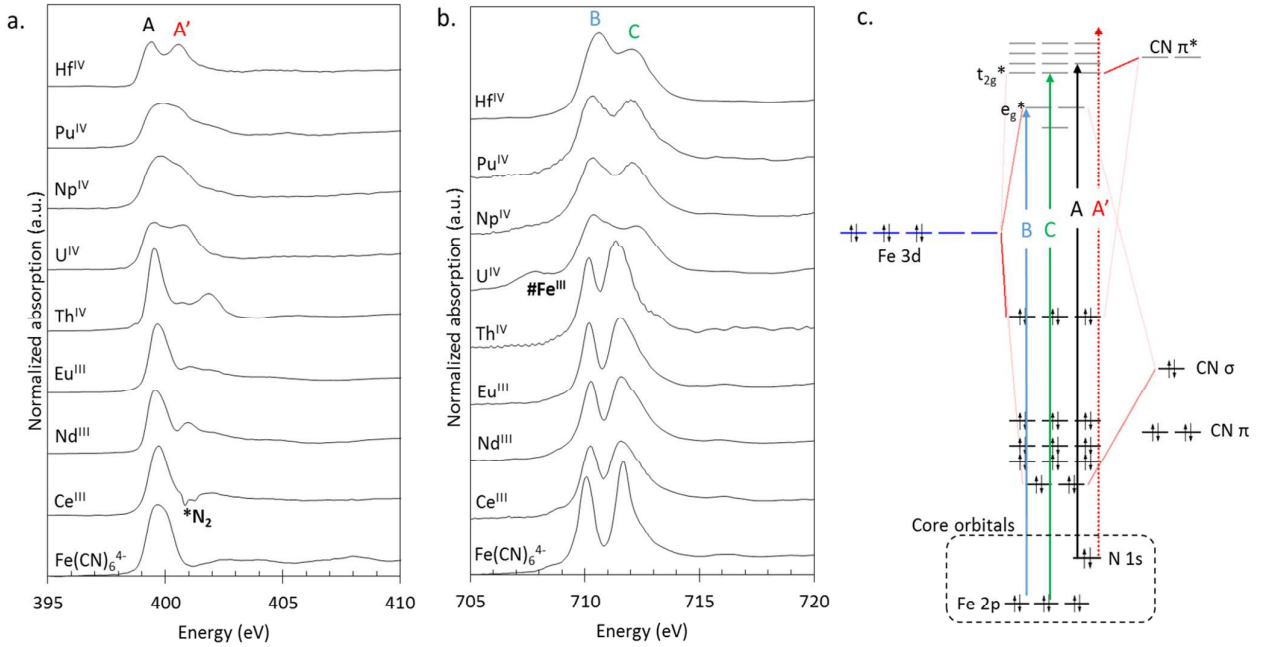

Figure 2 N K edge (**a.**) and Fe L_3 edge (**b.**) spectra for 5f and 4f PBAs, along with $K_4[Fe(CN)_6]$ and Hf PBA reference spectra. $*N_2$ indicates spurious spectral features due to molecular nitrogen contamination and $\#Fe^{III}$ a ferricyanide contamination in the air sensitive U^{IV}-PBA (transition to the e_g orbital in Fe^{III} complexes). **c.** Molecular orbital diagrams calculated by DFT calculation in a fixed geometry for $K_4[Fe(CN)_6]$ (interactions between Fe^{2+} and CN^- fragments also showing unoccupied MO's and the core hole orbital involved in the XAS process).

iron L_3 edges that the idealized electronic structure is disturbed. On one side, the π* and t_{2g}* MOs probed at the nitrogen N K edge are not observed as single peak but are split and/or enlarged. An intense secondary peak (A') is observed for 5f-PBA and the Hf-PBA, whereas for 4f-PBA's, the main peak A seems almost preserved as in $K_4[Fe(CN)_6]$ with only small secondary peaks arising between 401 eV and 403 eV. In the iron L_3 edges spectra, at least two spectral modifications can be noticed. First, the iron edge is clearly shifted to higher energy in comparison to the $[Fe(CN)_6]^{4-}$ L_3 edge spectrum. Second, both peaks B and C are enlarged and the relative intensity of peak B to peak C is reversed for U-PBA, Np-PBA, Pu-PBA and Hf-PBA. Overall, nitrogen and iron edge spectra follow the trend noticed from infrared and optical spectroscopies. In comparison to the $K_4[Fe(CN)_6]$ reference spectra, the ferrocyanide electronic structure is less modified in 4f-PBAs than in 5f-PBAs which tend to behave similarly to the Hf-PBA compound. DFT calculations and spectral simulation on Th-PBA demonstrated that the A' peak is due to a split in both π* and t_{2g}* MOs induced by a significant interaction with thorium 6d and 5f.[21] Extrapolating this phenomena to the remaining PBA spectra, a qualitative analysis can be proposed herein. First, from the A' peak intensity, it is clear that this π interaction with the 4f and/or 5d orbitals appears very weak in the Ln-PBA series. On the contrary, the cyano π* interaction with the hafnium 5d orbital is presumably very strong. This also seems to be the case for U-PBA, Np-PBA and Pu-PBA for which multiple spectral features are convoluted as a large absorption band. Moreover the A' peak shifts from 401.2 eV for Th-PBA to 400.3 eV for Pu-PBA. This behavior could be indicative and inline with the actinide 5f and 6d orbital contraction interactions with the cyano MOs probed at nitrogen K edge. This type of shift in actinide – ligand electronic structure has been predicted by theoretical calculations and/or experimentally measured using ligand K edge X-ray absorption spectroscopy.[22-24] However, because the electronic structures of actinide complexes involves both 6d and 5f orbitals in a narrow energy range (with variations along the series), it is often difficult to precisely distinguish spectral features and therefor, the electronic transitions to each type of MO. Moreover, the ferrocyanide building block involves covalent bonds between the iron 3d orbitals and the cyano MOs making the actinide cyano bond analysis even more intricate and complex. Hence, a reliable calculation of the electronic structure for a fully quantitative interpretation of this data set is daunting (the theoretical approach previously applied to reproduce the Th-PBA spectrum was limited to closed shell actinides). To overcome those issues and limitations, the N K edge spectra were analyzed using a curve fit based on constrained pseudo-Voight (p-V) and fixed step functions. The resulting curve fits, presented in Figure 3, are only used to understand changes in spectral features in a semi-quantitative manner. For instance, in agreement with previous work on the $K_4[Fe(CN)_6]$ electronic structure, a single pseudo Voight function (red line) is sufficient to model the N K edge spectrum of $K_4[Fe(CN)_6]$. The peak originates from convoluted transitions to the π* and t_{2g}* MOs (Figure 2.c, arrow A). For the other spectra, peak A is maintained with fixed energy parameters and only its amplitude fit. Thus, the amplitude of peak A can be then understood as composed of transitions to "undisturbed" ferrocyanide MOs. The secondary peaks (Figure 2.c, arrow A') arising at higher energy were modelled with two pseudo-Voight (blue lines). These peaks are assumed to originate from the cyano π* orbital interactions with lanthanide or actinide f and d orbitals, in accord to those observed in Th-PBA.[21] From this simple model, one can analyze lanthanide and actinide PBA from the p-V function areas. First, the area of peak A decreases for all the PBA samples in comparison to the $K_4[Fe(CN)_6]$ reference. This confirms that the p character of the cyano MOs is spread into another type of bonding. Within the 4f-PBA compounds, the area of peak A is maintained almost stable at 5.5 to 6.0 a.u. (normalized area unit) as well as the secondary peaks 2.5 to 2.8 a.u.. Hence, the number of f electrons does not influence the total peak area showing that the cyano MO splitting might only involve unoccupied 4f or 5d orbitals. From Th-PBA to Pu-PBA, the area of peak A decreases (5.4 to 3.2 a.u.) with a concomitant increase of the second peak area (compared to the 4f-PBA). This is well in line with a stronger 5f-6d orbital interaction with the cyano ligand in comparison to the 4f-5d.

The apparent decrease in the total area from Th-PBA to Pu-PBA also indicates a decrease in the p character in the cyano LUMOs. In this case, orbital mixing with actinide 5f and 6d might involve occupied orbitals, hence 5f or 6d electron charge transfer to the cyano ligand

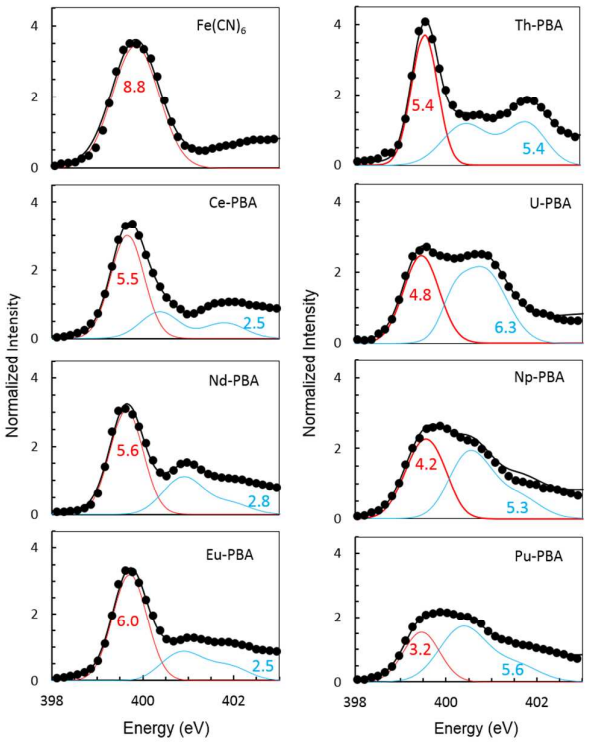

Figure 3 N K edge spectra in the near-edge region (Black circles) and fit (black line). The p-V functions in red correspond to the $K_4[Fe(CN)_6]$ reference energy, p-V functions in blue are additional contributions in the f-block PBA's spectra due to f orbital interactions with the cyano MOs. Fixed step functions are omitted for clarity. Numbers in red and blue are the corresponding p-V areas.

through a π back-bonding effect is very likely. Changes in a longer range scale observed at the iron L_3 edge spectra are consistent with this observation. The shape modifications of peak C (Figure 2b) for U, Np and Pu–PBAs translates this competitive π interaction between the two sides of the cyano bridge. This is also in line with the decrease in the ν_{CN} stretching frequencies (Figure 1b) that decrease as the number of 5f electron rises. Overall, the metal cyano bond in the 5f-PBAs appears to show more hints for a covalent properties in comparison to the 4f-PBAs (orbital mixing and charge transfer). Moreover, the similarities between 5f-PBA with the hafnium analog spectral features suggests a d-block like behavior of the actinides PBAs. The split of cyano π* orbitals and the strongly altered iron 3d orbitals are consistent with more covalent bonding between actinides and cyano ligands while these effects are much less intense for the lanthanide compounds. The ability of actinides to form π interactions with unoccupied cyano π* orbitals like d-block elements (whereas the lanthanide cyano bond remains mostly ionic) are likely to explain differences in optical properties. The isolated LnIII sites obstruct electronic exchange within the cyano ligand favoring a Robin and Day class 1 behavior whereas the more covalent bonds formed between An(IV) ions and the cyano ligand foster IVCT between iron and actinides to form Robin and Day class 2 colorful compounds.

This work was supported by French CEA/DEN/R-CHIM research program of Basic Research in Chemistry and the European IRSES program under HEXANE project (number 230807). This research was supported in part by the Director, Office of Science, Office of Basic Energy Sciences, Division of Chemical Sciences, Geosciences, and Biosciences (CSGB) Heavy Elements Chemistry program of the U.S. Department of Energy (DOE) under Contract Number DE-AC02-05CH11231 at Lawrence Berkeley National Laboratory (DKS). Beamline 11.0.2 at the ALS was supported in part by the aforementioned Division of CSGB Condensed Phase and Interfacial Molecular Sciences program of the U.S. DOE under Contract Number DE-AC02-05CH11231 at LBNL. This research used resources of the Advanced Light Source, which is a DOE Office of Science User Facility under Contract No. DE-AC02-05CH11231.

Conflicts of Interests

There are no conflicts to declare.

Notes and references

1. M. B. Robin, *Inorg Chem*, 1962, **1**, 337-&.
2. M. A. Arrio, P. Sainctavit, C. C. D. Moulin, T. Mallah, M. Verdaguer, E. Pellegrin and C. T. Chen, *J Am Chem Soc*, 1996, **118**, 6422-6427.
3. C. C. D. Moulin, F. Villain, A. Bleuzen, M. A. Arrio, P. Sainctavit, C. Lomenech, V. Escax, F. Baudelet, E. Dartyge, J. J. Gallet and M. Verdaguer, *J Am Chem Soc*, 2000, **122**, 6653-6658.
4. G. Paul, Y. Prado, N. Dia, E. Riviere, S. Laurent, M. Roch, L. Vander Elst, R. N. Muller, L. Sancey, P. Perriat, O. Tillement, T. Mallah and L. Catala, *Chem Commun*, 2014, **50**, 6740-6743.
5. F. X. Bu, M. Hu, W. Zhang, Q. Meng, L. Xu, D. M. Jiang and J. S. Jiang, *Chem Commun*, 2015, **51**, 17568-17571.
6. T. Matsuda, M. Takachi and Y. Moritomo, *Chem Commun*, 2013, **49**, 2750-2752.
7. M. Shatruk, C. Avendano and K. R. Dunbar, *Prog Inorg Chem*, 2009, **56**, 155-334.
8. G. W. Beall, D. F. Mullica, W. O. Milligan, J. Korp and I. Bernal, *Acta Crystallogr B*, 1978, **34**, 1446-1449.
9. D. F. Mullica, W. O. Milligan and J. D. Oliver, *Inorg Nucl Chem Lett*, 1979, **15**, 1-5.
10. W. O. Milligan, D. F. Mullica and H. O. Perkins, *Inorg Chim a-Article*, 1982, **60**, 35-38.
11. D. F. Mullica, H. O. Perkins, E. L. Sappenfield and D. Leschnitzer, *Acta Crystallogr C*, 1989, **45**, 330-331.
12. D. F. Mullica, E. L. Sappenfield and H. O. Perkins, *J Solid State Chem*, 1989, **78**, 301-306.
13. F. Goubard and A. Tabuteau, *J Solid State Chem*, 2002, **167**, 34-40.
14. F. Goubard and A. Tabuteau, *Struct Chem*, 2003, **14**, 257-262.
15. I. Bonhoure, C. Den Auwer, C. C. D. Moulin, P. Moisy, J. C. Berthet and C. Madic, *Can J Chem*, 2000, **78**, 1305-1317.
16. G. Dupouy, I. Bonhoure, S. D. Conradson, T. Dumas, C. Hennig, C. Le Naour, P. Moisy, S. Petit, A. C. Scheinost, E. Simoni and C. Den Auwer, *Eur J Inorg Chem*, 2011, DOI: 10.1002/ejic.201001004, 1560-1569.
17. T. Dumas, M. C. Charbonnel, I. A. Charushnikova, S. D. Conradson, C. Fillaux, C. Hennig, P. Moisy, S. Petit, A. C. Scheinost, D. K. Shuh, T. Tyliszczak and C. Den Auwer, *New J Chem*, 2013, **37**, 3003-3016.
18. H. J. Nilsson, T. Tyliszczak, R. E. Wilson, L. Werme and D. K. Shuh, *Anal Bioanal Chem*, 2005, **383**, 41-47.
19. T. Tyliszczak, H. J. Nilsson, L. Werme and D. K. Shuh, *Geochim Cosmochim Ac*, 2005, **69**, A599-A599.
20. R. K. Hocking, E. C. Wasinger, F. M. F. de Groot, K. O. Hodgson, B. Hedman and E. I. Solomon, *J Am Chem Soc*, 2006, **128**, 10442-10451.
21. T. Dumas, D. Guillaumont, C. Fillaux, A. Scheinost, P. Moisy, S. Petit, D. K. Shuh, T. Tyliszczak and C. Den Auwer, *Phys Chem Chem Phys*, 2016, **18**, 2887-2895.
22. S. G. Minasian, J. M. Keith, E. R. Batista, K. S. Boland, J. A. Bradley, D. L. Clark, S. D. Conradson, S. R. Daly, S. A. Kozimor, W. W. Lukens, R. L. Martin, D. K. Shuh, T. Tyliszczak, G. L. Wagner and P. Yang, *Abstr Pap Am Chem S*, 2012, **243**.
23. S. G. Minasian, J. M. Keith, E. R. Batista, K. S. Boland, D. L. Clark, S. D. Conradson, S. A. Kozimor, R. L. Martin, D. E. Schwarz, D. K. Shuh, G. L. Wagner, M. P. Wilkerson, L. E. Wolfsberg and P. Yang, *J Am Chem Soc*, 2012, **134**, 5586-5597.
24. S. G. Minasian, J. M. Keith, E. R. Batista, K. S. Boland, D. L. Clark, S. A. Kozimor, R. L. Martin, D. K. Shuh and T. Tyliszczak, *Chem Sci*, 2014, **5**, 351-359.

Electronic Supporting Informations : Electronic structure of f-element Prussian Blue analogs determined by soft X-ray absorption spectroscopy.

Thomas Dumas*[a], Dominique Guillaumont[a], Philippe Moisy[a], David K. Shuh[b,c], Tolek Tyliszczak[c], Pier Solari[d] and Christophe Den Auwer[a,e]

[a] CEA, Nuclear Energy Division, Radiochemistry and Process Department, 30207 Bagnols-sur-Cèze, France. E-mail: thomas.dumas@cea.fr.
[b] Chemical Sciences Division, Lawrence Berkeley National Laboratory, Berkeley, CA 94720, USA.
[c] Advanced Light Source Division, Lawrence Berkeley National Laboratory, LBNL, Berkeley, CA 94720, USA.
[d] Synchrotron SOLEILL'Orme des Merisiers, Saint-Aubin, BP 48F-91192, Gif-sur-Yvette Cedex, France
[e] Université Côte d'Azur, CNRS, Institut de Chimie de Nice, UMR 7272, 06108 Nice, France
Electronic Supplementary Information (ESI) available: [Hafnium ferrocyanide structural description]. See DOI: 10.1039/x0xx00000x

The hafnium ferrocyanide compound local structure was characterized by Extended X-ray Absorption fine Structure performed at both the iron K edge and the Hafnium L3 edge. The spectra were recorded the soleil synchrotron beamline MARS equipped with a water-cooled Si(220) double crystal horizontal focusing monochromator (DCM), as well as two large water-cooled reflecting and vertical focusing mirrors, set with Pt strips at 3.1 mrad. All the measurements were recorded in fluorescence mode using a 13-element high-purity germanium solid-state detector, and were performed at room temperature. Data processing was carried out with the Athena code. After energy calibration, the E0 energy was set at the maximum of the absorption edge. For all samples, this maximum confirmed the redox state + IV for hafnium and +II for iron. The EXAFS signal was extracted by subtracting a linear pre-edge background and a combination of cubic spline functions for atomic absorption background, and then normalizing. These signals were fitted using model clusters derived from the luthetium ferrocyanide crystal structures by use of the Artemis code. Both iron and hafnium EXAFS spectra were fitted together with the same metrical parameter as performed previously for the actinides ferreocyanide structural determination. [1, 2]

The k^3 EXAFS weighted and corresponding fourrier transformed are presented Figure S1. The obtained values for interatomic distances and fit parameters are displayed in table S1.

Table S1: Fit parameter for the hafnium ferrocyanide

	dFe-C (Å)	dC-N (Å)	dAn/Hf–O (Å)	dAn/Hf-N(Å)	θ (°)
Hf(IV)/Fe(II) R-factor : 3.35% Amp_{Fe}=0.6 ΔE_{0Fe}=-6.8eV Amp_{Hf}=0.8 ΔE_{0Hf}=7.8eV	1.88(1) σ^2=0.004Å²	1.16(1) σ^2=0.004Å²	2.15(1) σ^2=0.009Å²	2.24(1) σ^2=0.002Å²	169° ± 1°

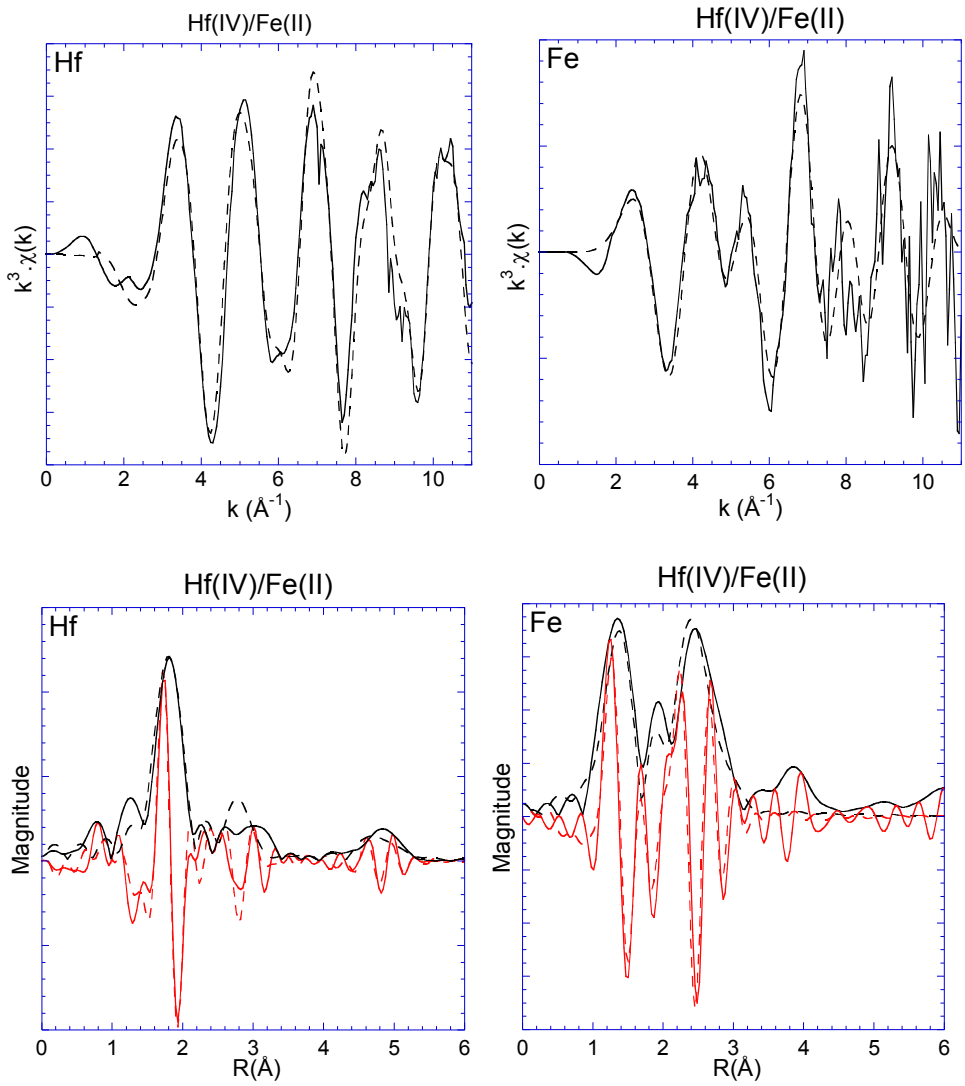

Figure S1: top k^3 weighted iron K edge (left) and hafnium L3 edge (right) and corresponding fit (dotted lines). Bottom corresponding Fourier transform magnitude and imaginary par (red) for the iron K edge (left) and hafnium L3 edge (right).

References:

1. G. Dupouy, I. Bonhoure, S. D. Conradson, T. Dumas, C. Hennig, C. Le Naour, P. Moisy, S. Petit, A. C. Scheinost, E. Simoni and C. Den Auwer, *Eur J Inorg Chem*, 2011, DOI: 10.1002/ejic.201001004, 1560-1569.
2. T. Dumas, M. C. Charbonnel, I. A. Charushnikova, S. D. Conradson, C. Fillaux, C. Hennig, P. Moisy, S. Petit, A. C. Scheinost, D. K. Shuh, T. Tyliszczak and C. Den Auwer, *New J Chem*, 2013, **37**, 3003-3016.